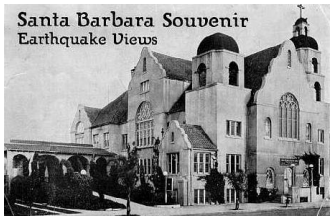

4th IASPEI / IAEE International Symposium:

Effects of Surface Geology on Seismic Motion

August 23–26, 2011 · University of California Santa Barbara

STRONG GROUND MOTIONS IN THE SAPPORO METROPOLITAN AREA DURING THE 2010 CENTRAL ISHIKARI EARTHQUAKE

Michiko SHIGEFUJI
Hokkaido University
N13W8 Kita-ku, Sapporo
Japan

Tsutomu SASATANI
Hokkaido University
N13W8 Kita-ku, Sapporo
Japan

Nobuo TAKAI
Hokkaido University
N13W8 Kita-ku, Sapporo
Japan

ABSTRACT

The Sapporo metropolitan area is located on a deep sedimentary basin in the Ishikari depression, the western part of Hokkaido, Japan. A moderate-size shallow earthquake (Mw 4.6) occurred on December 2, 2010 beneath the southern part of Sapporo city. Peak ground acceleration and velocity at the nearest site with the epicentral distance of about 1 km are about 340 cm/s/s and 13 cm/s, respectively. The displacement waveforms at the near stations (< 10 km) show clear near-field term motions. The record sections of velocity waveforms along a profile in the NNW direction from the epicenter show conspicuous later phases after the direct P- and S-wave. First, we re-determined the source parameters (the hypocenter position, focal mechanism, rise time, and seismic moment) using the near-field records by modelling the observed waveforms. Next, we investigate the observed record sections to understand effects of sedimentary layers on ground motion. The synthetic waveforms by 1-D simulation using the velocity structure model after AIST and the re-determined source parameters reproduce the observed later phases; these later phases are the multi-reflected wave inside the whole of sedimentary layers. These suggest that the source parameters re-determined in this study and the AIST velocity structure along the profile are reasonable.

INTRODUCTION

On December 2, 2010 at 6:44 (JST), a moderate-size shallow earthquake occurred beneath the southern part of Sapporo city in the central Ishikari region; here, we call this event the 2010 Central Ishikari earthquake. The magnitude of this event, according to Japan Metrological Agency (JMA), is Mj=4.6. This event is the largest one since the observation had started in this area. This event caused slight damage such as breakage of structures and slide of sloping ground surface around the epicenter. Sapporo District Meteorological Observatory (2010) reported that strong shaking occurred around the epicenter; seismic intensity at that area is 4 to 5 lower.

The Sapporo metropolitan area is located on a deep sedimentary basin in the Ishikari depression, the western part of Hokkaido, Japan. The population of Sapporo-city is about 2 million, and the high-rise buildings with a height of over 100m have increased recently. Sapporo city government carried out the seismic refraction and reflection surveys, and microtremor surveys [Sapporo city, 2002, 2003, 2004, 2005], in order to construct the 3-D velocity structure model of the Sapporo basin. Recently the National Institute of Advanced Industrial Science and Technology (AIST) developed 3-D velocity structure model of the Ishikari and Yūfutsu sedimentary basins integrating existing these data [Yoshida *et al.*, 2007].

We obtained a lot of strong motion data from the 2010 Central Ishikari earthquake. These data provide a good opportunity for studying effects of sedimentary layers on ground motion. The observed data show the interesting features such as near-field motions at the near-field stations and conspicuous later phases after the direct P- and S-wave at the far-field stations. In this paper, we make a preliminary study of these observed records. First, we re-determine the source parameters (the hypocenter location, focal mechanism, rise time and seismic moment) using the near-field records by modelling the observed waveforms. Next, we investigate the observed record section along the NNW profile to understand the generation mechanism of the conspicuous later phases at the far-field stations.

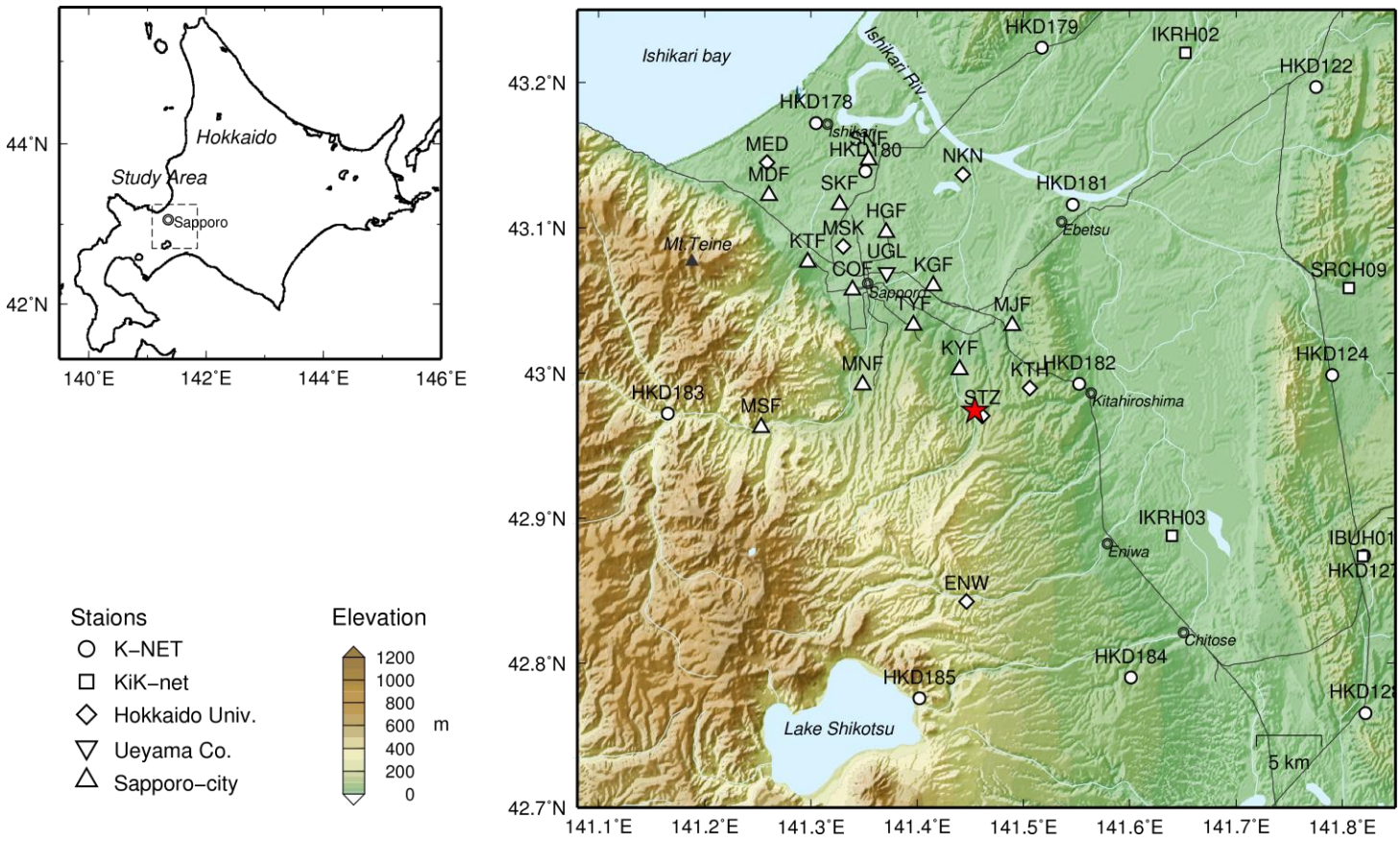

Fig. 1. Map showing the study area and locations of stations used in this study. A red star shows the epicenter determined by Ichiyanagi et al. (2011).

STRONG GROUND MOTIONS

In the Sapporo metropolitan area we have moderately dense strong motion observation stations (Fig. 1). These stations recorded ground motion during the 2010 Central Ishikari earthquake. We use strong motion records from K-NET, KiK-net of NIED (National Research Institute for Earth Science and Disaster Prevention), the Seismic Intensity Network of Sapporo city, Ueyama Corporation, and Hokkaido University.

Figure 2 (a) shows the spatial distribution map of peak ground acceleration (PGA) values in the south-west Hokkaido; PGA is the largest value of NS and EW components. Figure 2 (b) shows the attenuation relationship of PGA. An empirical attenuation relationship of PGA by Si and Midorikawa (1999) is also shown as the reference relationship. The PGA value at the nearest station STZ is the largest one (see Fig. 3) which exceeds one standard deviation of the empirical relationship. The PGA values at larger distances greater than 10 km decay rapidly compared with the empirical relationship. This feature was also observed during the 2004 Rumoi earthquake (Mw 5.7; Maeda and Sasatani, 2009). Figure 2 (c) shows the spatial distribution map of JMA (Japan Meteorological Agency) seismic intensity in the study area. The seismic intensity at STZ is 4.4. This suggests that the seismic intensity around the epicenter is about 4 or more; slight damage occurred around the epicenter during this earthquake [Sapporo District Meteorological Observatory, 2010].

Figure 3 shows observed acceleration, velocity, and displacement waveforms at STZ. The velocity and displacement waveforms are obtained by integration of the acceleration waveforms in the frequency domain. In this process we apply a high-pass filter with a cut-off frequency of 0.1 Hz [Saito, 1978]. The PGA and PGV (peak ground velocity) are about 340 cm/s/s and 13 cm/s on the EW components; the PGA value is larger than the empirical value as mentioned above. The velocity S-waveform on the EW component shows a simple, one-cycle sine-wave shape with a period of about 0.5 s. We consider this wave corresponds to the far-field S-waveform. Based on this fact, we assume the Bell-shaped moment rate function with a width of 0.5 s in the later simulation. The displacement waveforms are strange compared with the acceleration and velocity waveforms. The NS and EW components show long-period

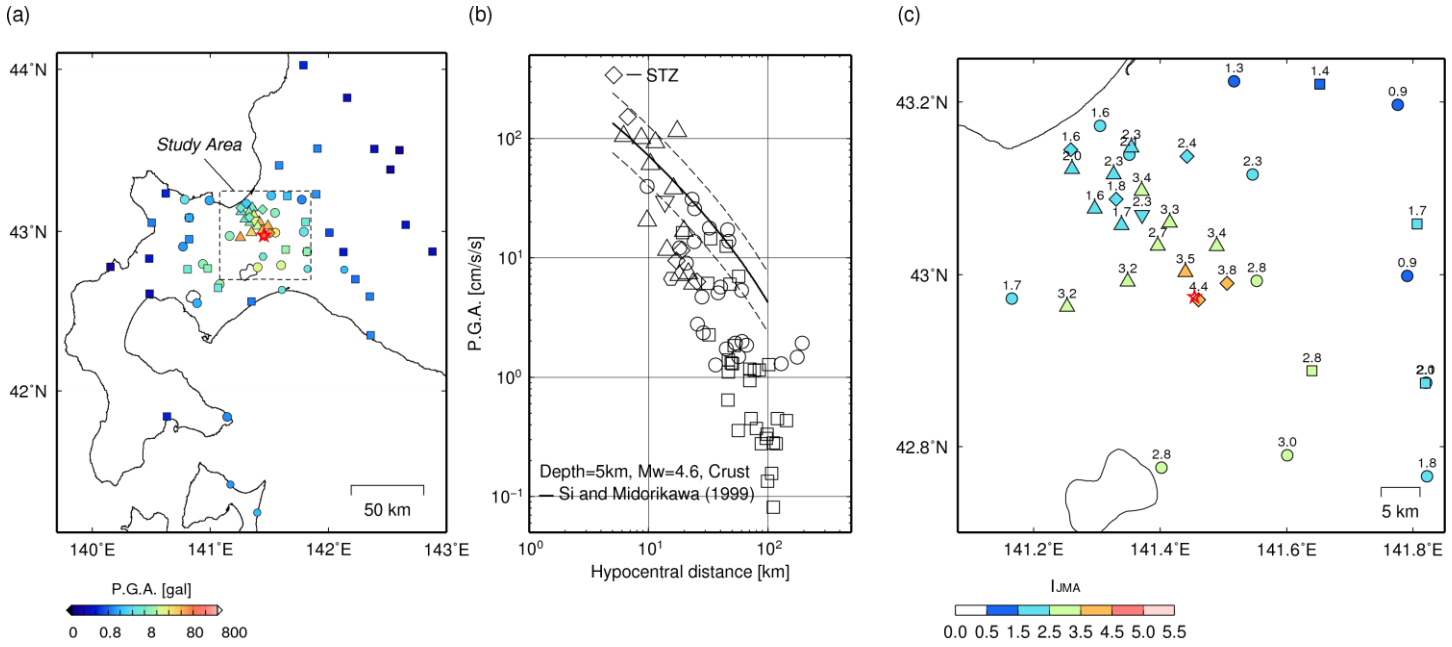

Fig. 2. (a) Spatial distribution map of PGA values in the south-west Hokkaido. The study area is indicated by a dotted square. (b) Attenuation relationship of PGA values. The empirical relationship (solid curve) proposed by Si and Midorikawa (1999) is also shown. (c) Spatial distribution map of JMA seismic intensities in the study area.

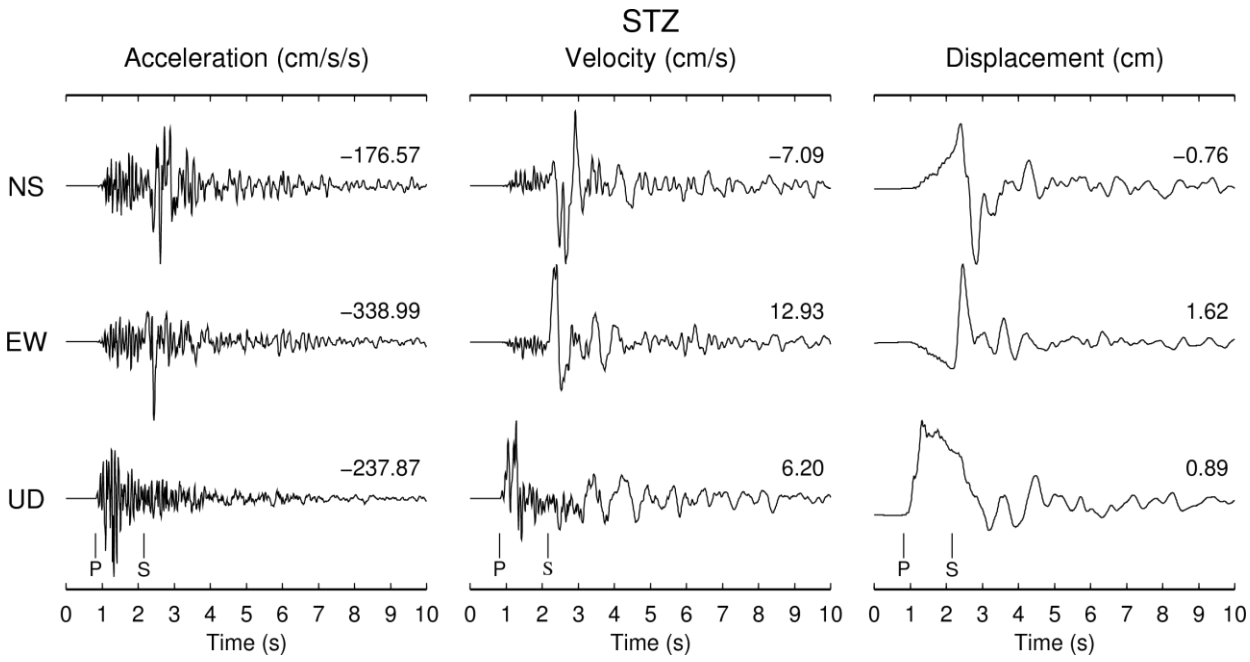

Fig. 3. Observed records at the nearest station STZ. Left: acceleration, Middle: velocity, and Right: displacement waveforms. Amplitudes are normalized; numbers attached to each trace show the maximum amplitudes.

motion during P-wave arrival to S-wave arrival; the UD component shows a pulse waveform with long duration (about 2 s). These peculiar waveforms may be attributed to the near-, intermediate- and far-field terms [Aki and Richards, 1980]; the displacement field due to a point shear dislocation source is given by the sum of these three terms. A few studies analyzed these peculiar waveforms and retrieved important source information [ex., Jiao *et al.*, 1995; Kosuga, 1996]. In the next section we analyze near-field records from the 2010 Central Ishikari earthquake to check how important information is retrieved from the analysis.

ANALYSIS OF THE NEAR-FIELD RECORDS

Figure 4 shows the epicenters and focal mechanisms of the 2010 Central Ishikari earthquake determined by previous studies. Both epicenters determined by ICY and JMA using P- and S-wave arrival-time data are close to the STZ station. This is natural because the STZ data is included in the hypocenter determination and the S-P time at STZ is very short as shown in Fig. 3. The focal mechanisms of F-net and JMA2 are determined by modelling far-filed long-period waveforms, but those of ICY and JMA1 are determined from P-wave initial motion data. These mechanisms show thrust type mechanisms with a small difference in orientation of nodal planes.

As shown in Fig. 3, the displacement waveforms at the nearest station STZ are strange compared with the acceleration and velocity waveforms; this is considered to be due to overlapping of the near-, intermediate- and far-field terms. First of all, we examine whether the source parameters of previous studies explain these peculiar waveforms at STZ. Synthetic displacement waveforms are calculated by using the discrete wavenumber (DWN) method [Bouchon, 1981; Takeo, 1985] and they are compared with the observed waveforms. In the calculation, we use the epicenters and focal mechanisms shown in Table 1, but fix the focal depth of 5 km, seismic moment of 8.43E+15 Nm, and Bell-shaped moment rate function with a width of 0.5 s. The 1-D velocity structure around STZ is constructed based on the 3-D velocity structure model of the Ishikari sedimentary basin by AIST [Yoshida *et al.*, 2007]. Figure 5 shows a comparison of the observed displacement waveforms with the synthetic ones. All synthetic UD-component waveforms roughly explain the observed ones. However all synthetic NS and EW-component waveforms do not explain the observed ones. This indicates that these epicenters and focal mechanisms are not reasonable. Although these focal mechanisms are similar as shown in Fig. 4, the synthetic waveforms differ strongly. This indicates that the synthetic waveforms at a near-field station are considerably sensitive to the focal mechanism.

Next we re-determine the epicenter and focal mechanism of the 2010 Central Ishikari earthquake by modelling the near-filed records at eight stations shown in Fig. 4. Observed displacement waveforms at these stations (distance less than 10 km from STZ) are also peculiar as shown in Fig. 8 left. We make a two-step grid search. The aim of the first step is to estimate a rough position of the epicenter based on the STZ records using the circular array search; the array configuration is shown in Fig. 6 (a). We calculate the synthetic waveforms at STZ for each epicenter in the array using the ICY focal mechanism; the other parameters are the same as used in the previous calculation. The results are shown in Fig. 7. We can see that the probable epicenter lies in the back azimuth range of 150~180 degree. Based on this result, we make the second step search; the configuration of the checkerboard grid search is shown in Fig. 6 (b). In this case, the synthetic waveforms are calculated at eight stations; the 1-D velocity structure used in calculation for each station is assumed based on the AIST 3-D velocity structure model. The mechanism search is also done for each grid point (a trial epicenter) by changing the dip angle (the search range of 50-65) and the rake angle (the search range of 60-120), referring to the F-net and ICY focal mechanisms; however the strike angle is fixed to be 7.5 (middle value of the two mechanisms). The optimum epicenter and focal mechanism are shown in Fig. 6 (b). Figure 8 shows a comparison of the observed displacement waveforms with the synthetic ones for the optimum solution. An agreement between the observed and synthetic waveforms is fairly good except the station HKD182. Finally we estimate the seismic moment by comparing the maximum amplitudes of the observed and synthetic waveforms. The source parameters obtained in this study are summarized in Table 2.

Table 1. Source parameters of the previous studies. For ICY, F-net, JMA1, and JMA2, see captions in Fig. 4.

	Latitude	Longitude	Depth [km]	Mw	Mo [Nm]	Fault plane 1			Fault plane 2		
						strike	dip	rake	strike	dip	rake
ICY	42.97	141.46	5.1	-	-	6	53	73	213	39	111
F-net	42.98	141.44	5.0	4.6	8.43E+15	9	66	104	158	28	62
JMA1	42.98	141.44	3.0	-	-	177	34	61	30	61	108
JMA2	42.98	141.44	10.0	4.5	6.26E+15	353	49	85	180	41	96

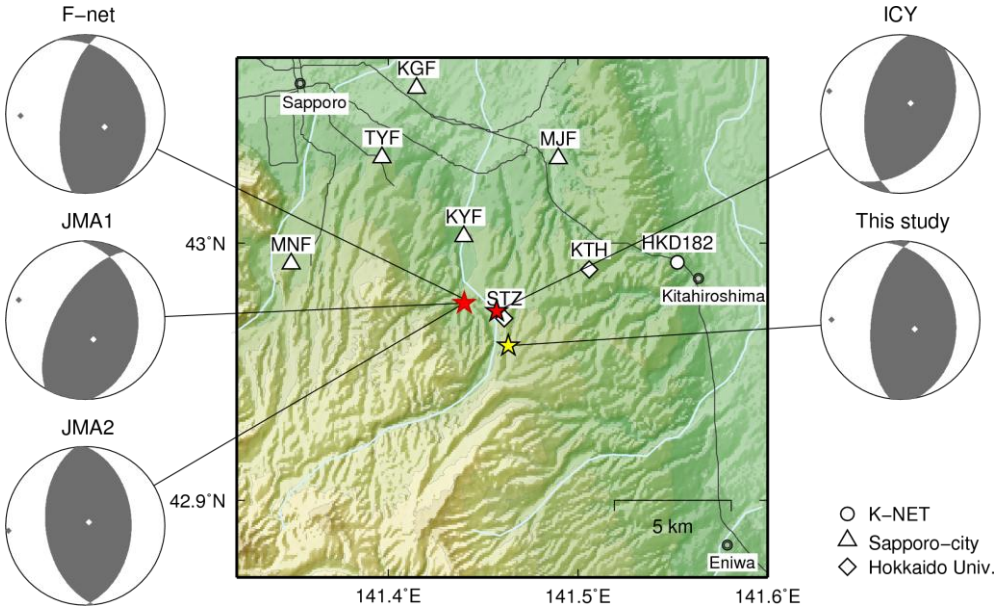

Fig. 4. Location of stations used in analysis of the near-field records. Also shown are the epicenters and focal mechanisms of the 2010 Central Ishikari earthquake determined in the previous studies and this study: these parameters are shown in Table 1 and 2. F-net: moment tensor solution by NIED, JMA1: P-wave initial motion solution by *JMA, JMA2: moment tensor solution by JMA, ICY: P-wave initial motion solution by Ichiyanagi et al. (2011), and This study: solution determined here by modelling the near-filed records. Focal mechanisms are shown by using the upper hemisphere projection.*

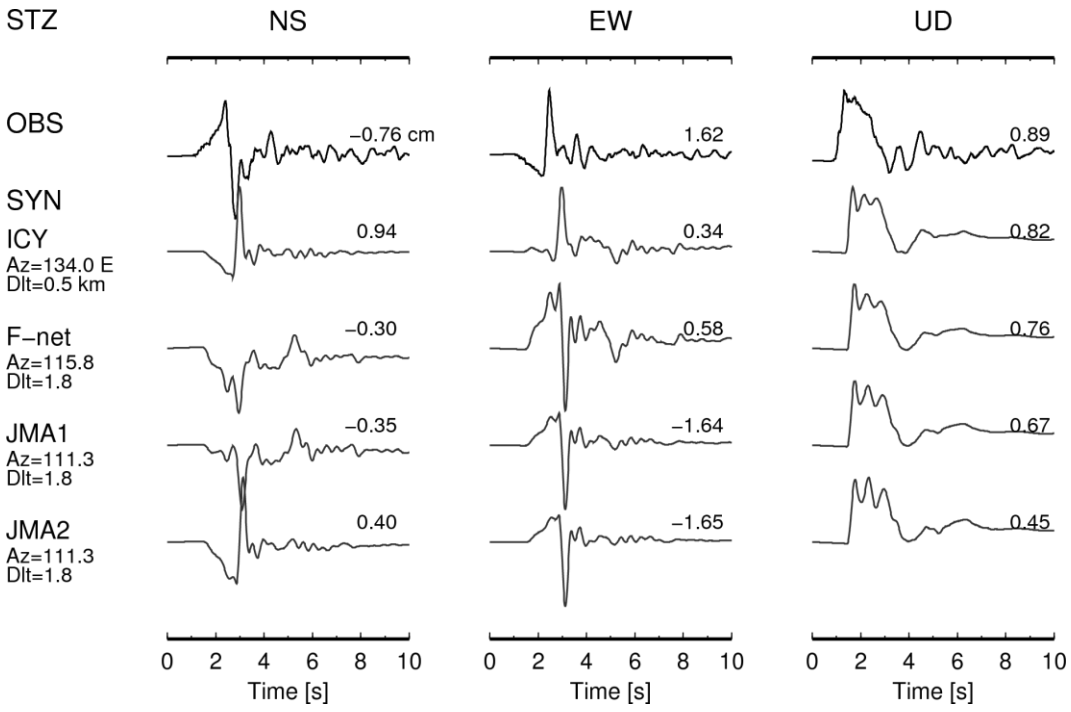

Fig. 5. Comparison of the observed displacement waveforms with the synthetic ones at STZ. The synthetic waveforms are calculated for the source parameters of previous studies.

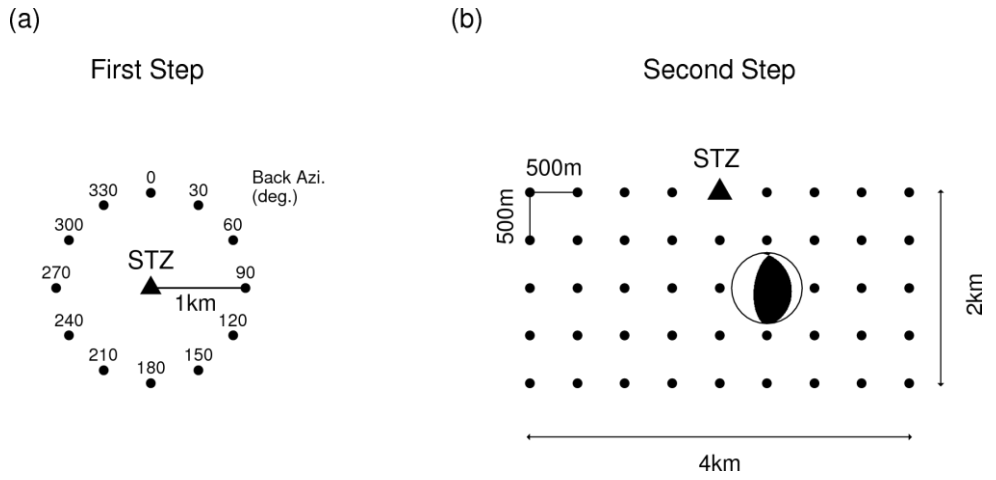

Fig. 6. (a) Configuration of the circular array search. Numbers indicate the back azimuth. (b) Configuration of the checkerboard grid search. The focal mechanism determined is located at the optimum epicenter.

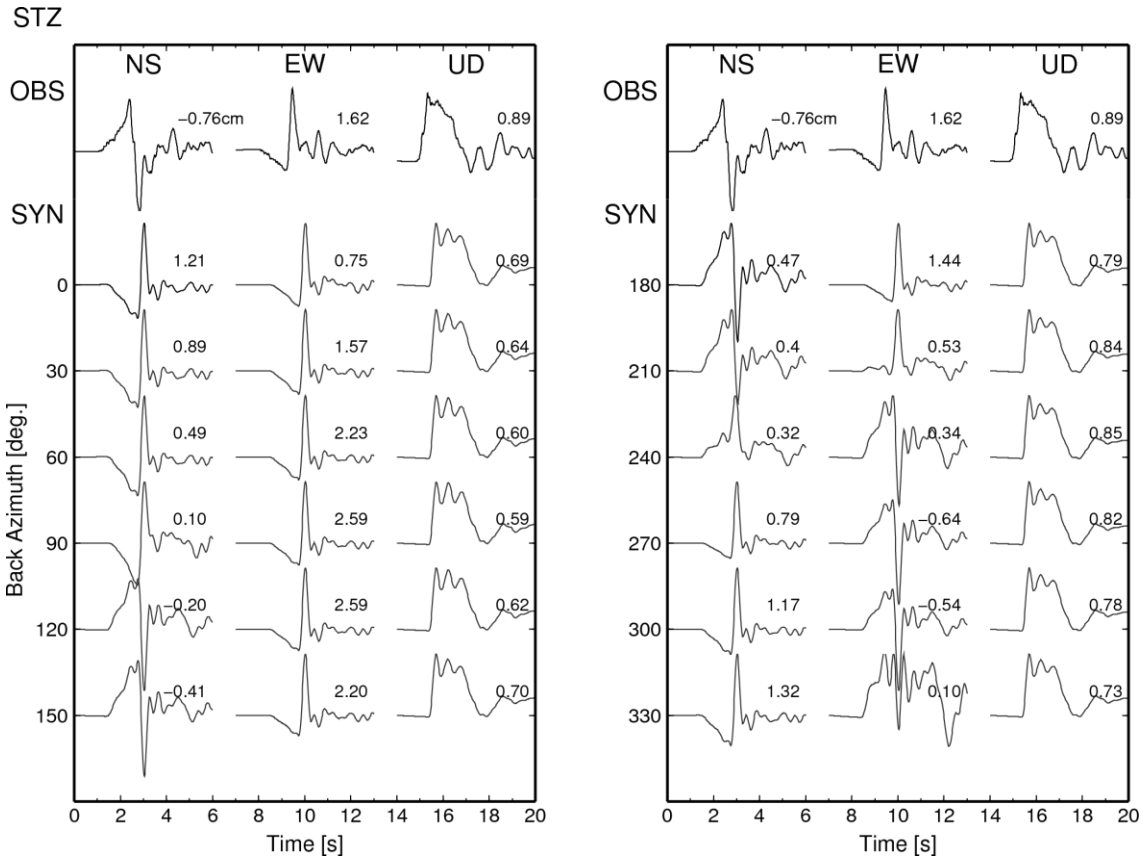

Fig. 7. Comparison of the observed displacement waveforms with the synthetic ones at STZ. The synthetic waveforms for each point in the array are calculated by using the mechanism solution of ICY, the seismic moment of F-net and the focal depth of 5km.

Table 2. Source parameters determined in this study

Latitude	Longitude	Depth [km]	Mo [Nm]	strike	dip	rake	Rise time [s]
42.96	141.46	5.0	6.5E+15	7.5	60	100	0.5

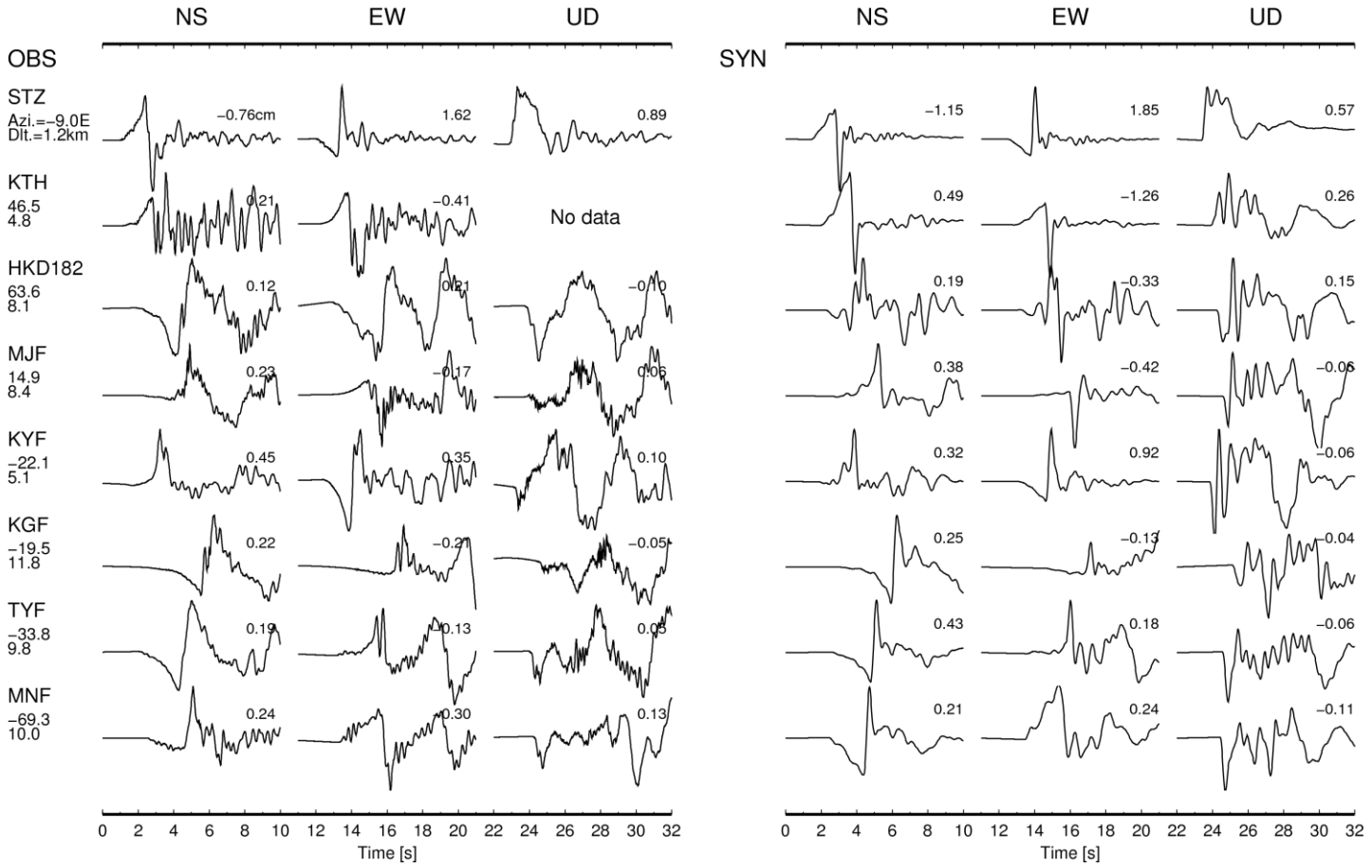

Fig. 8. Comparison of the observed displacement waveforms (left) and the synthetic ones (right) at the near 8 stations. The synthetic waveforms are calculated for the optimum epicenter and focal mechanism. The UD-component at KTH was missed due to ill condition of instrument. The epicenter-to-station azimuth (degrees) and the epicentral distance (km) are attached to station code. Amplitudes are normalized; numbers attached to each trace show the maximum amplitudes.

ANALYSIS OF THE FAR-FIELD RECORDS

Finally we analyze the far-filed records to understand effects of sedimentary layers on ground motion. Figure 9 (a) shows the depth to the top of the seismic basement in the study area; this figure is constructed from the 3-D velocity structure model by AIST [Yoshida *et al.*, 2007]. P- and S-wave velocities of the basement are 5.78km/s and 3.40km/s, respectively. The maximum depth is about 7km at the north of the epicenter. We select a profile A-A' as shown in Figure 9 (a); the profile length is about 30km. As shown in a vertical cross-section of the profile A-A' in Fig. 9 (b), the seismic basement is roughly flat and the depth is about 4km. Undulation in sedimentary layers is not so strong.

Figure 10 shows a record section of the observed velocity waveforms along the profile A-A'. The NS and EW components are rotated into the radial and transverse components using the hypocenter position determined in this study (Table 2). The direct P- and S-waves are easily identified on the vertical and transverse components as shown by P0 and S0 lines. The P0 and S0 lines indicate an apparent velocity of about 6 km/s and 3 km/s, respectively; these values are nearly the same as P- and S-wave velocities of the seismic basement. We can identify conspicuous later phases at about 4 s after the direct S-wave on the transverse component section; these phases appear at distances greater than 12 km and the travel time are indicated by S1 line that is parallel to S0 line. On the radial component section similar later phases after the direct S-wave are identified although it is not so clear. We can also identify conspicuous later phases at about 2 s after direct P-wave on the vertical component section; these phases appear at distances greater than 17 km, and the travel times are indicated by P1 line that is parallel to P0 line.

It is interesting to understand the generation mechanism of the direct and later phases mentioned above. We make a 1-D simulation using DWN method [Bouchon, 1981; Takeo, 1985]. The velocity structure used in the DWN simulation is shown in Fig. 9 (c), and the

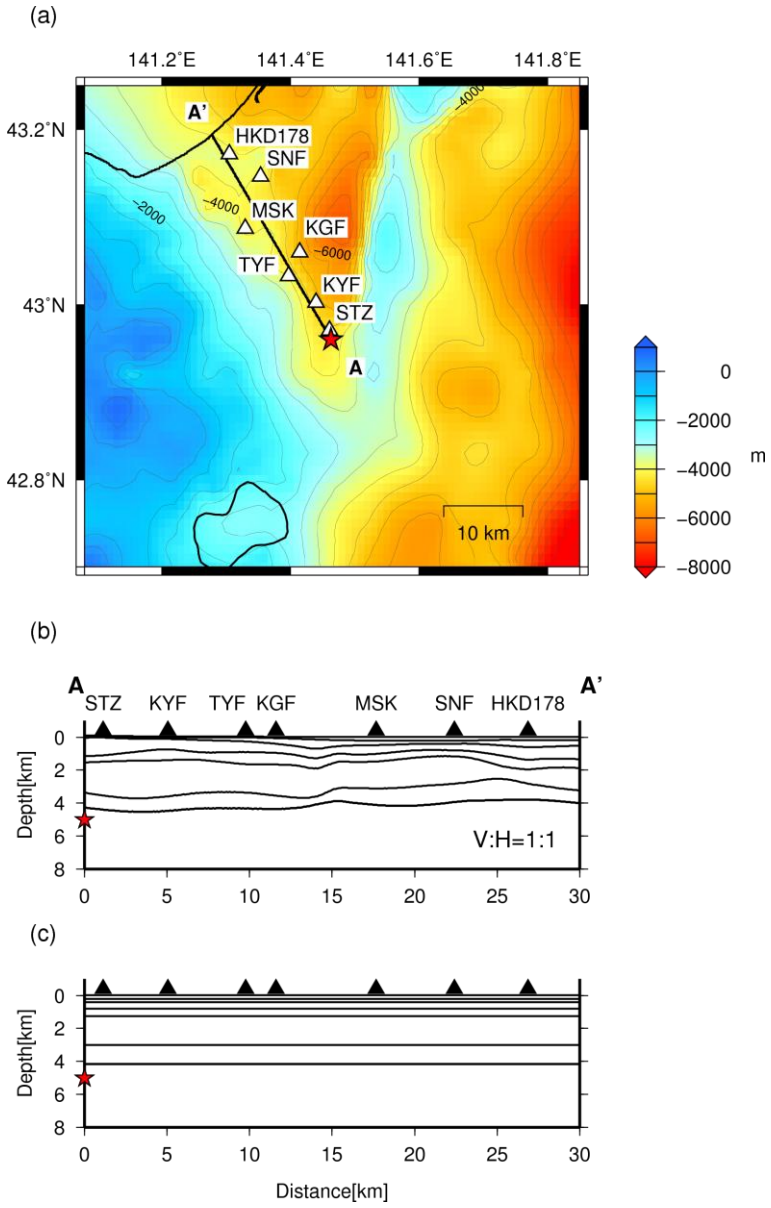

Fig 9. (a) Location map of the profile A-A' and stations selected for a waveform examination. Depth to the top of the seismic basement after AIST [Yoshida et al., 2007] is also shown. (b) Vertical cross-section of the velocity structure along the profile A-A'.(c) Assumes 1-D velocity structure for Discrete Wavenumber simulation. Material parameters of the velocity structure are shown in Table 3.

Table 3. Material parameters of the velocity structure used in DWN simulation

Vp [km/s]	*Vs* [km/s]	Density [g/cm^3]	Depth [km]	*Qp*	*Qs*
1.76	0.400	1.98	0.000	50	50
2.09	0.722	1.98	0.227	80	80
2.62	1.196	2.06	0.404	100	100
3.21	1.725	2.27	0.742	150	150
4.07	2.350	2.41	1.166	200	200
5.42	3.131	2.57	2.902	300	300
5.78	3.400	2.77	4.110	340	340

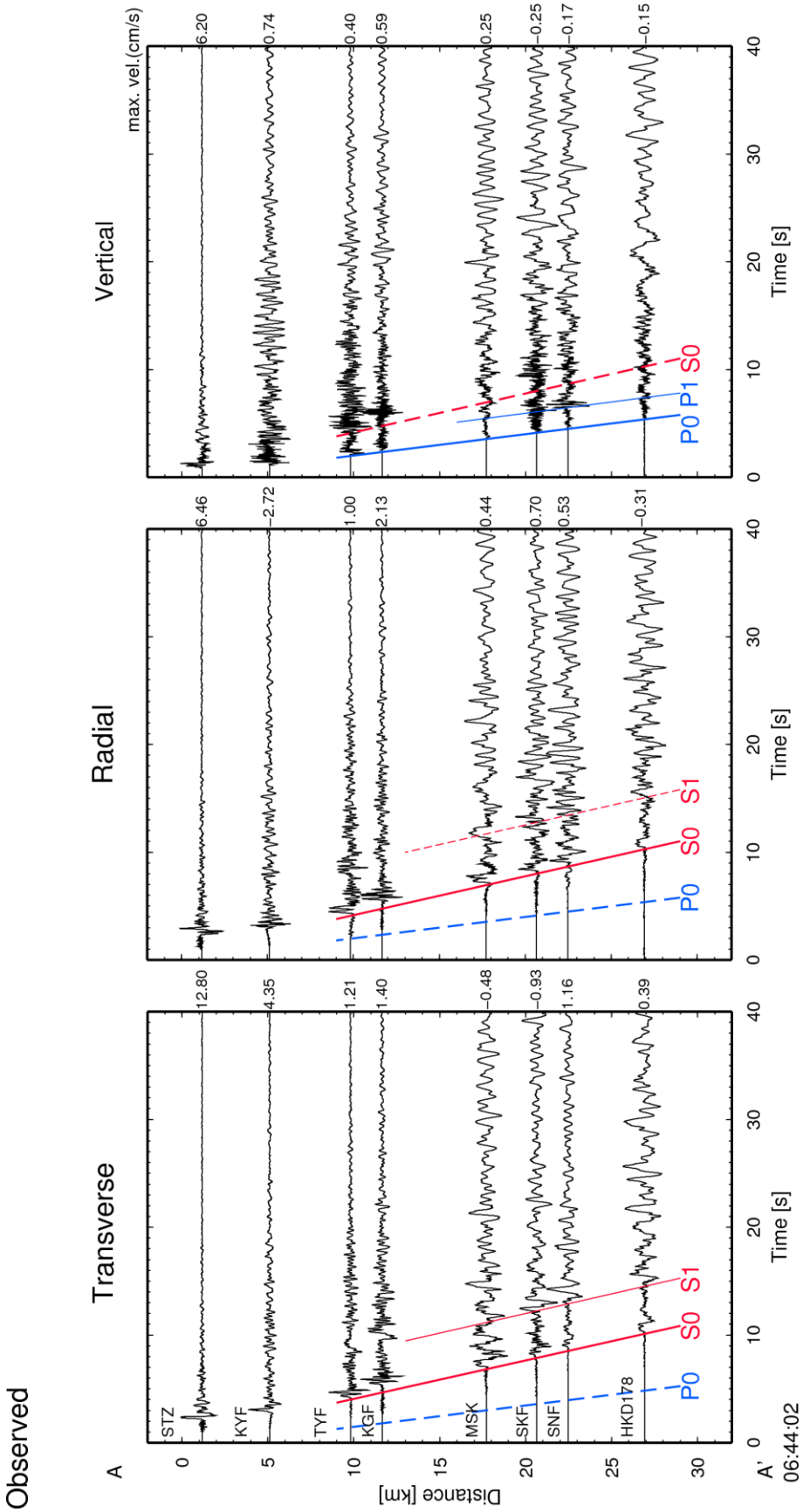

Fig. 10. Observed record sections along the profile A-A'. For P0, P1, S0 and S1, see captions in Fig. 11.

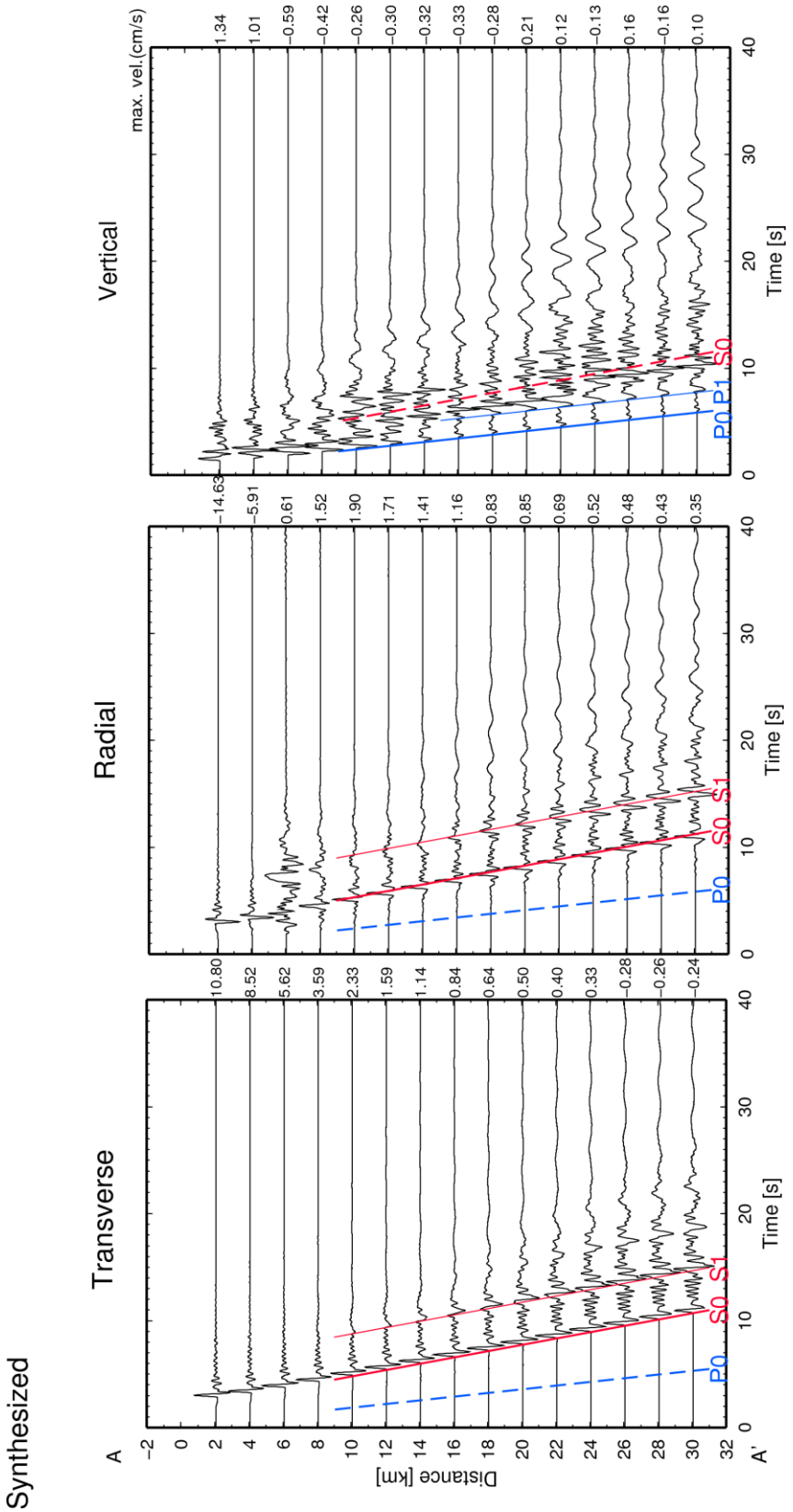

Fig. 11. Synthetic record sections along the profile A-A'. P0 and P1 lines are the travel-time lines for the direct and reflected P-waves; S0 and S1 lines are the travel-time lines for the direct and reflected S-waves. The ray paths for these waves are shown in Fig. 12. Solid lines are obtained based on the observed phases, and dotted lines are referred from the lines on the other components.

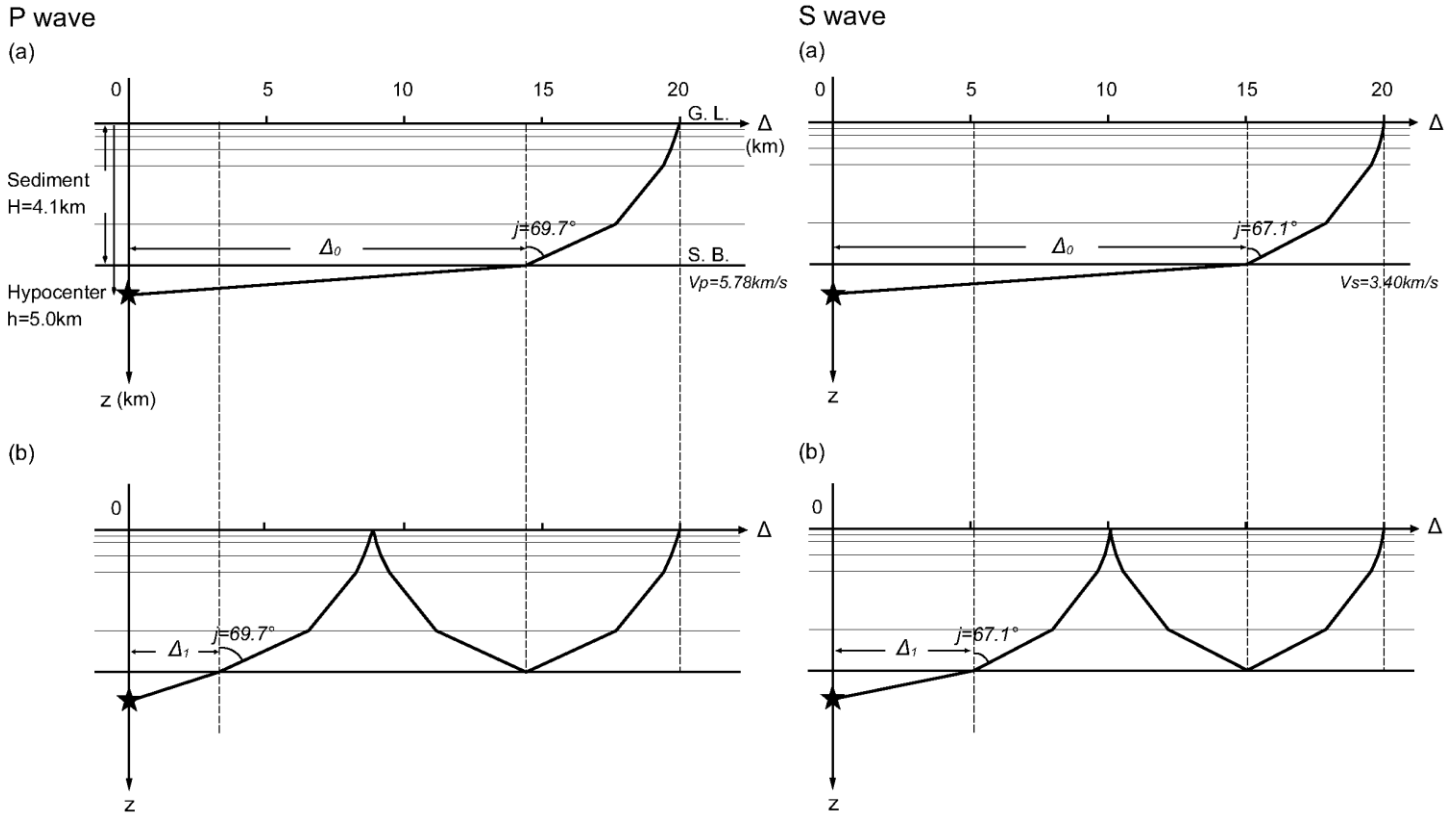

Fig. 12. Left: Ray paths for the direct (a) and multi-reflected (b) P-waves. Right: Ray paths for the direct (a) and multi-reflected (b) S-waves. These figures are constructed based on the ray path equations by Ben-Menahem and Singh [1981; formulas (7.248)-(7.250)] and the velocity structure shown in Fig. 9 (c). The ray paths toward the 20km point on the profile A-A' are shown.

material parameters of the velocity structure are listed in Table 3. A station array is located from 2 to 30 km at intervals of 2 km along the profile A-A'. We use the source parameters determined in this study (Table 2) assuming a point source. Figure 11 shows the synthetic record sections along the profile A-A'. The travel times of the direct P- and S-wave are indicated by P0 and S0 lines. The observed later phases after the direct S-wave on the transverse components and the direct P-wave on vertical components are well reproduced by the simulation; these are indicated by S1 and P1 lines. We confirm that general features of the observed waveforms mentioned above are well reproduced by the 1-D simulation. Although it is difficult from the DWN simulation to know the wave paths for the direct and later phases, we confirm that the focal depth of 5 km is the key to generation of the strong later phases; a tentative simulation for a depth of 6 km generate no strong later phases.

We found the ray path equations for the direct and later phases in a book by Ben-Menahem and Singh (1981). Figure 12 shows the ray paths for the direct and later phases along the profile A-A' constructed based on their results [formulas (7.248) – (7.250) in p. 518]. The later phase is a multi-reflected wave inside the whole of sedimentary layers. From the ray paths, we easily understand that the apparent velocities of S0 and S1 correspond to S-wave velocity of the seismic basement and that those of P0 and P1 correspond to P-wave velocity of the seismic basement. The velocity structure determines the time difference between the direct and multi-reflected wave; the time difference between S0 and S1 is 3.9 s, and that between P0 and P1 is 1.6 s; these values are nearly the same as observed ones. The ray paths in Fig. 12 also show that the shortest distance where the multi-reflected wave appears is about 15 km for S-wave and is about 17 km for P-wave; the synthetic waveforms shown in Fig. 11 verify this. From above considerations, we conclude that the synthetic waveforms well reproduce the observed ones. This implies that the source parameters determined in this study and the velocity structure along the profile A-A' are reasonable.

CONCLUSION

We re-determined the source parameters of the 2010 Central Ishikari earthquake using the near-field records by modelling the observed near-filed term waveforms. Next, we investigated the observed record section along the NNW profile to understand the genera-

tion mechanism of the conspicuous later phases at the far-field stations. The synthetic waveforms calculated by using the re-determined source parameters and the AIST velocity structure along the profile well reproduced the observed later phases. From this fact, we concluded that the source parameters re-determined in this study and the AIST velocity structure along the NNW profile are reasonable. However, this study is a preliminary one because the target area was limited and 1-D simulation was used. We are planning to make 3-D simulation to verify the AIST velocity structure of the Sapporo metropolitan area.

ACKNOWLEDGEMENTS

We would like to thank NIED for providing the strong motion data by KiK-net, K-NET, also the source parameter by F-net; the seismic intensity network of Sapporo city, Ueyama Corporation, and Hokkaido University for providing the strong motion data; JMA for providing the source parameter. We would particularly like to thank Masahiro Ichiyanagi for providing strong motion data and source parameter. Most figures were drawn by GMT (Generic Mapping Tools, Wessel and Smith, 1998). This research was partially supported by the Ministry of Education, Science, Sports and Culture, Grants-in-Aid for Scientific Research, 212410440, 2011.

REFERENCES

Aki, K. and P. G. Richards [1980], "*Quantitative Seismology*", W. H. Freeman and Company, pp. 932.

Ben-Menahem A. and S. J. Singh [1981], "*Seismic waves and source*s", Springer-Verlag GmbH, NY, pp. 1108.

Bouchon, M. [1979], "Simple method to calculate Green's functions for elastic layers media", Bull. Seismol. Soc. Am., 71, pp. 989-971.

Ichiyanagi, M., T. Yamaguchi, R. Azuma, M. Takada, K. Kuroi, T. Yamada, J. Miyamura, and H. Takahashi [2011], "Seismic activity of the December 3, 2010 Sapporo earthquake (MJMA4.6)", Japan Geoscience Union Meeting 2011 (in Japanese).

Kosuga, M. [1996], Near-field moment tensor inversion and stress field in northeastern Japan", Tohoku university, Ph.D. thesis.

Maeda, T. and T. Sasatani [2004],"Strong ground motions from an Mj 6.1 inland crustal earthquake in Hokkaido, Japan: the 2004 Rumoi earthquake", Earth Planets Space, Vol. 61, pp. 689-701.

Saito, M. [1978], "An automatic design algorithm for band selective recursive digital filters", Geophys. Exploration, pp. 240–263 (in Japanese with English abstract).

Sapporo District Meteorological Observatory [December 3, 2010], "Reports of the earthquake in the central Ishikari region on December 2", Press release, http://www.jma-net.go.jp/sapporo/news/2010/sp_press101203.pdf (in Japanese).

Sapporo city [2002, 2003, 2004, 2005], "Estimation of Subsurface Structures of Ishikari basin", http://www.hp1039.jishin.go.jp /kozo/eqkozo frm.htm.

Si, H. and S. Midorikawa [1999], "New attenuation relationships for Peak ground acceleration and velocity considering effects of faults type and site condition", J. struct. Constr. Eng. AIJ, 523, pp. 63-70 (in Japanese with English abstract).

Takeo, M. [1985], "Near-field synthetic seismograms taking into accunt the effects of an elastic attenuation on seismograms caused by asedimentary layer-, Meterol. Geophys., 36, pp. 235-257 (in Japanese with English abstract).

W. Jiao, T. C. Wallace, and S. L. back [1995], "Evidence for static displacements from the June 9, 1994 deep Bolivian earthquake", Geophysical Res. Letters, Vol. 22, No. 16, pp. 2285-2284.

Wessel, P., Smith, W. H. F. [1998], "New, improved version of the Generic Mapping Tools released", EOS Trans. AGU 79, 579.

Yoshida, K., M. Yoshimi, H. Suzuki, M. Morino, F. Takizawa, H. Sekiguchi, and H. Horikawa [2007], "3D velocity structure model of the Ishikari and Yūfutsu sedimentary basins", Annual report on active fault and paleoearthquake researches, No. 7, pp.1-29 (in Japanese with English abstract).